Sound production due to main-flow oriented vorticity-nozzle interaction in absence of a net swirl

Hirschberg, L.; Bake, F.; Hulshoff, S.J.

DOI
10.2514/6.2022-3055

Publication date
2022

Document Version
Final published version

Published in
28th AIAA/CEAS Aeroacoustics 2022 Conference

Aeroacoustics Conferences
June 14-17, 2022, Southampton, UK
28th AIAA/CEAS Aeroacoustics 2022 Conference

10.2514/6.2022-3055

Sound production due to main-flow oriented vorticity-nozzle interaction in absence of a net swirl

L. Hirschberg*
Imperial College London, London SW7 1AY, UK

F. Bake†
Bundesanstalt für Materialforschung und -prüfung (BAM), Unter den Eichen 87, 12205 Berlin, Germany

S. J. Hulshoff‡
Delft University of Technology, Kluyverweg 1, 2629HS Delft, The Netherlands

The downstream acoustic response due to the interaction of main-flow oriented vorticity with a choked nozzle in a swirl-free flow was experimentally demonstrated. The response was obtained by means of impulsive radial air injection in the pipe upstream from the nozzle. The resulting downstream acoustic data are shown to obey a scaling rule that differs, from the one for swirl-nozzle interaction, which according to the literature is proportional to the square of the swirl number. In contrast, here evidence is presented that points to the scaling of main-flow oriented vorticity noise with the cross-sectional average of the square of the transversal velocity at the throat divided by the square of the critical sound speed.

Nomenclature

c	=	sound speed, $\mathrm{m}\cdot\mathrm{s}^{-1}$
f_1	=	upstream-pipe quarter-wavelength oscillation , Hz
f_c	=	low-pass filter cutt-off frequency, Hz
f_{ref}	=	pistonphone reference frequency, Hz
M	=	Mach number
$\dot{m}$	=	axial mass-flow rate at the nozzle throat, $\mathrm{kg}\cdot\mathrm{s}^{-1}$
$\dot{m}^*$	=	critical-nozzle axial mass-flow rate at the nozzle throat in absence of swirl, $\mathrm{kg}\cdot\mathrm{s}^{-1}$
$\delta\dot{m}_{\mathrm{st}}$	=	swirl induced change in axial mass-flow rate, $\mathrm{kg}\cdot\mathrm{s}^{-1}$
$\dot{m}_\theta$	=	unsteady tangentially injected mass-flow rate, $\mathrm{kg}\cdot\mathrm{s}^{-1}$
p	=	pressure, Pa
$\Delta p_2'$	=	vorticity induced difference in downstream acoustic signal, Pa
$\lvert p'_{\mathrm{ref}}\rvert$	=	pistonphone calibration pressure, dB
R	=	radius, m
S_D	=	Swirl number, –
t	=	time, s
T	=	temperature, K
Δx_{inj}	=	distance between unsteady-injection port and nozzle inlet, m
u	=	velocity, $\mathrm{m}\cdot\mathrm{s}^{-1}$
V_{set}	=	volume of upstream settling chamber m^3
V_{inj}	=	volume of unsteady-injection reservoir, m^3
α_{crt}	=	fit coefficient for pressure dependence of injection mass-flow rate, $\mathrm{kg}\cdot\mathrm{s}^{-1}\cdot\mathrm{Pa}^{-1}$
γ	=	specific heat ratio, $\gamma \equiv c_p/c_v$
ρ	=	density, $\mathrm{kg}\cdot\mathrm{m}^{-3}$

*Research Associate, Imperial College London, Department of Mechanical Engineering, 58 Princes Gate, South Kensington, London SW7 1AY, UK, AIAA Member.

†Head of Division for Acoustic and Electromagnetic Methods, Department of Non-destructive Testing, Bundesanstalt für Materialforschung und -prüfung (BAM), Unter den Eichen 87, 12205 Berlin, Germany

‡Assitant Professor, Faculty of Aerospace Engineering, Delft University of Technology, Kluyverweg 1, 2629HS Delft, The Netherlands.

τ_{inj} = unsteady-injection injection time, s
$\langle \dots \rangle$ = cross-sectional average

Subscripts

1 = subscript for variables upstream of the choked-nozzle
2 = subscript for variables downstream of the choked-nozzle
th = subscript indicates variables at the throat
r = subscript indicates radial component
inj = subscript indicates upstream unsteady-injection variables
tan = subscript indicates tangential injection
rad = subscript indicates radial injection
amp = subscript indicates amplitude
θ = subscript indicates azimuthal/tangential component

Superscript

$'$ = indicates perturbation
$*$ = critical

I. Introduction

The interaction of vortices with a choked nozzle is a source of indirect combustion noise, commonly referred to as vorticity noise [1]. Its radiation to the environment could be a significant source of noise pollution. Its radiation back into the combustion chamber can result in spurious self-sustained pressure pulsations or thermo-acoustic instability. Vorticity noise driven self-sustained pressure pulsation are particularly problematic in large solid rocket motors [2, 3].

King and Bake [4] developed a cold-gas experimental setup for the study of voricity noise in isolation, i.e., in the absence of combustion. In Kings' and Bake's experiment, an impulsively-generated vortex oriented in the main-flow direction interacts with a choked convergent-divergent nozzle [4]. The vortex was generated upstream from the nozzle by means of tangential injection of air through a fast-switching valve. However, the setup used by Kings and Bake [4] had two major shortcomings [5–7]:

1) The acoustic signal recorded downstream from the nozzle was obscured by acoustic reflections at the downstream open-pipe termination
2) The tangentially injected mass-flow rate, $\dot{m}_\theta$, was undetermined.

Here, for the first time, the experimentally-obtained downstream acoustic response deduced to be due to the interaction of main-flow oriented vorticity with a choked convergent-divergent nozzle in absence of a net swirl is reported.

II. Scaling laws for steady flows

Using an improved version of this setup, which mitigated the above enumerated deficiencies, Hirschberg et al. [5] found that the downstream acoustic signal, p_2', produced due to the interaction of the main-flow oriented vortex referred to as swirl, scales with the square of the impulsively-injected tangential mass-flow rate $\dot{m}_\theta$.

For steady flows, Dutton [8] demonstrated that this axial mass-flow rate reduction effect increase quadratically with the swirl number, S_D, defined by Dutton [8] as follows

$$S_D \equiv \frac{\langle u_{\theta,\text{th}} \rangle}{c^*} \tag{1}$$

where $\langle u_{\theta,\text{th}} \rangle$ is the cross-sectional average azimuthal velocity at the nozzle throat, and c^* the critical speed of sound of the flow. In the absence of swirl, the mass-flow rate at the choked nozzle throat is $\dot{m}^* = \rho^* c^* \pi R_{\text{th}}^2$, where R_{th} is the radius at the throat and ρ^* the critical density. Using a quasi-cylindrical modeling approach [9, 10], an equation relating

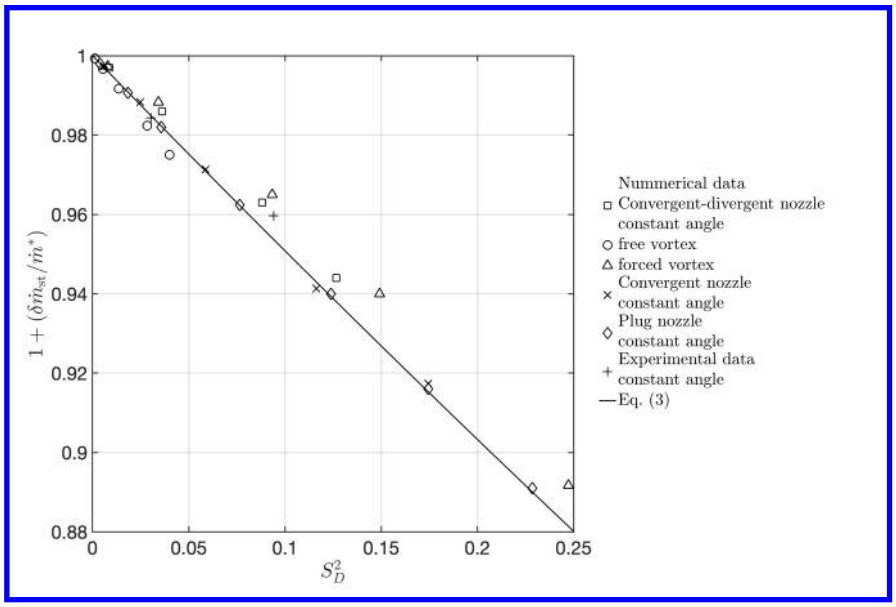

Fig. 1 Data reported by Dutton [8] compared to the theoretical quasi-cylindrical steady flow model Eq. (3).

$u_{\theta,\mathrm{th}}/c^*$ to the relative reduction of the axial mass-flow rate of a choked-nozzle flow due to the presence of the swirl in the nozzle throat can be found:

$$\frac{\delta\dot{m}_{\mathrm{st}}}{\dot{m}^*} \equiv \frac{\dot{m}_{\mathrm{st}} - \dot{m}^*}{\dot{m}^*} \tag{2}$$

Taking for the sake of tractability $u_{\theta,\mathrm{th}}$ to be uniform, and subsequently applying quasi-cylindrical modeling, yields

$$\frac{\delta\dot{m}_{\mathrm{st}}}{\dot{m}^*} = \left(1 - \frac{\gamma-1}{\gamma+1} S_D^2\right)^{\frac{\gamma+1}{2(\gamma-1)}} - 1 \tag{3}$$

where $\gamma = 1.4$ is the heat-capacity ratio of dry air [7]. In Fig. 1, numerical simulation and experimental data of steady-state swirl-nozzle interaction reported by Dutton [8] for different profiles of the azimuthal velocity $u_{\theta,\mathrm{th}}$ are compared to Eq. (3), for various nozzle geometries and azimuthal velocity distributions. One observes that, in spite of assuming a non-physical uniform $u_{\theta,\mathrm{th}}$, for small values of S_D^2 as is done here, the quasi-cylindrical model has remarkably good predictive value.

The reduction in mass flow is believed to be due to the reduction of stagnation enthalpy available to drive the flow through the nozzle for given stagnation enthalpy. This reduction is caused when kinetic energy has to be provided for the elongation of the main-flow oriented vortex during ingestion by the nozzle. This effect also occurs in the absence of a net swirl, whenever main-flow oriented vorticity is ingested by the nozzle. Ergo, in first approximation, the authors suggest that $S_D^2 = \langle u_\theta \rangle^2 / c^{*2}$ in Eq. (3) can be replaced by the cross-sectional average of the square of the transversal velocity at the nozzle throat divided by the square of the critical speed of sound:

$$\kappa^2 \equiv \frac{\left\langle u_{\theta,\mathrm{th}}^2 + u_{r,\mathrm{th}}^2 \right\rangle}{c^{*2}} \tag{4}$$

where $u_{r,\mathrm{th}}$ is the radial velocity. This is a generalization of the result obtained by Carpenter [11] to include the effect of a radial velocity component, which should be valid for steady or quasi-steady flows. For small values of κ in axially-symmetric swirl flows, substitution of S_D by κ in Eq. (3) results in to the general result derived by Carpenter [11]. The axial vortex type referred to as "constant angle" by Dutton [8], corresponds to the assumption of uniform azimuthal velocity used to derive Eq. (3), in which case $S_D^2 = \kappa^2$. One should note that without this proposed modification, Eq. (3) could not predict any mass flow reduction in the absence of net swirl.

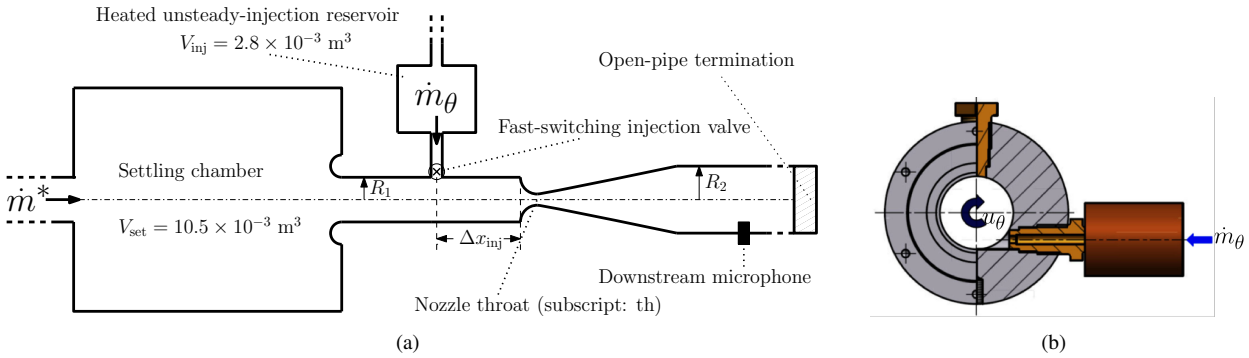

Fig. 2 (a) Sketch of the experimental setup. (b) Convergent-injection nozzle and fast-switching valve system in the tangential injection configuration (retouched version of figure in Ref. [5]).

III. Experiments

Assuming $S_D \propto \dot{m}_\theta$, Hirschberg et al. [5, 6] inferred that the interaction of a net non-zero swirl change with a choked nozzle reduces the axial mass-flow rate through the nozzle by an amount $\delta\dot{m}$ relative to $\dot{m}^*$, the mass flow without swirl at constant reservoir conditions. When swirl is ingested $\delta\dot{m} < 0$, which causes an acoustic expansion wave to be emitted downstream from the nozzle. As swirl is evacuated from the nozzle $\delta\dot{m} > 0$, which causes a compression acoustic wave to propagate downstream from the nozzle. Hirschberg et al. [5–7] chose to call this: sound production due to swirl-nozzle interaction.

This response was obtained by means of impulsive radial air injection in the pipe upstream from the choked convergent-divergent nozzle. In Fig. 2(a), a sketch of the experimental setup used to obtain the response is shown. The authors note that the setup is a variant of the one used by Hirschberg et al. [5] for their swirl-nozzle interaction experiments. Specifically, the modification consisted of plugging the tangential-injection port and attaching the convergent injection nozzle and fast-switching valve system into a separate threaded hole for radial injection. In Fig. 2(b), a sketch of the unsteady injection system in the tangential injection configuration is shown (the radial injection hole is shown plugged). The distance between the injection port of radius $R_{inj} = 1.25$ mm, and the nozzle inlet Δx_{inj}, could be set at either 85 mm or 185 mm. Design details about the fast-switching injection valve can be found in [12], and about how it was operated in [4]. The injection valve was connected to a $V_{inj} = 2.8 \times 10^{-3}$ m^3 radial-injection reservoir at pressure p_{inj} by means of a 3 m long hose with an inner diameter of 10 mm. Static calibration with a Bronkhorst F-203AV linear resistance flow meter [5, 7] was used to determine the relationship between the injection reservoir pressure p_{inj} and the injected mass flow m_{inj}. For a choked injection valve, this was found to be[5]

$$\dot{m}_{inj} = \alpha_{crt} p_{inj} \tag{5}$$

where $\alpha_{crt} = 6.676 \times 10^{-9}$ kg $\cdot$ s^{-1} $\cdot$ Pa^{-1}. The pipe section of radius, $R_1 = 15$ mm, upstream from the nozzle was 340 mm long. Upstream from its bellmouth inlet was a settling chamber with volume, $V_{set} = 10.5 \times 10^{-3}$ m^3. A Bronckhorst F-203AV linear resistance flow controller upstream from the settling chamber inlet was used to establish a stationary non-swirling axial choked-nozzle base flow, with a mass-flow rate of $\dot{m}^* = 1.19 \times 10^{-2}$ kg $\cdot$ s^{-1}. The contraction ratio of the nozzle was $R_1/R_{th} = 16$, with $R_{th} = 3.75$ mm. The wall of the upstream pipe and nozzle inlet formed a right angle. The nozzle's divergent section was 250 mm long, and led to a 25 m downstream section of radius $R_2 = 20$ mm. A GRAS 40BP 1/4" ext. polarized pressure microphone was mounted flush in its walls, calibrated using a Brüel & Kjaer model 4228 pistonphone at $|p'_{ref}| = 123.92$ dB and $f_{ref} = 251.2$ Hz, at a distance 1150 mm downstream from the nozzle throat. This 25 m downstream section made the reflection-free recording of vorticity noise possible for ca. 140 ms after the downstream-travelling, vorticity-noise generated acoustic wave passed to microphone. As was done by Hirschberg et al. [5]; a low-pass filter with frequency $f_c = 234$ Hz was applied to suppress the acoustic signal due to the quarter-wavelength oscillation in the upstream-pipe segment caused by direct sound due to the opening of the injection valve.

Radial air injection into the swirl-free stationary base flow was done using the fast-switching valve for a duration of $\tau_{inj} \simeq 25$ ms. This was repeated 100 times every 3 s. The resulting acoustic signal was phase averaged using the procedure described by Kings and Bake [4]. The authors note that although the opening of the injection valve was not p_{inj} dependent; Hirschberg et al. [5] found that its closing was marginally influenced by p_{inj}.

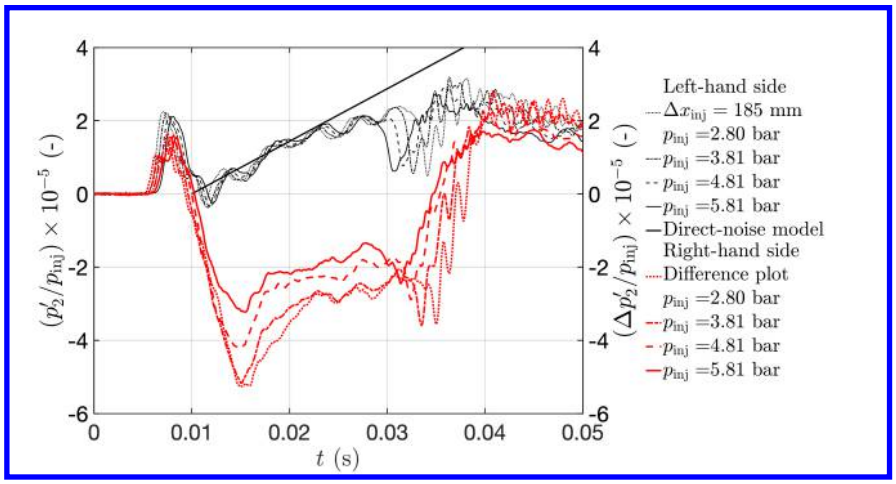

Fig. 3 Left-hand vertical axis: the downstream measured acoustic signal due to radial injection at Δx_{inj} = 185 mm, compared to the direct-noise model Eq. (10). Right-hand vertical axis: difference in downstream acoustic signal, $\Delta p_2' \equiv (p_2')_{\Delta x_{inj}=85\ mm} - (p_2')_{\Delta x_{inj}=185\ mm}$, between the Δx_{inj} = 85 mm and Δx_{inj} = 185 mm configurations.

It is assumed that radial injection induces an adiabatic compression in the reservoir. Since injection takes only a short time, the variation in total mass-flow through the convergent injection nozzle is negligible compared with $\dot{m}_{inj}$. Using a linearized integral mass balance, in linear approximation for small changes in p_1, one obtains

$$\frac{V_{set}}{c_1^2}\frac{dp_1}{dt} = \dot{m}_{inj}. \tag{6}$$

where p_1 and c_1 are the reservoir pressure and speed of sound upstream from the nozzle, respectively. Assuming a quasi-steady response of the nozzle to an adiabatic increase of upstream reservoir pressure, p_1, one finds the following relative increase of mass flow:

$$\frac{\dot{m}_1{}'}{\dot{m}_1} = \frac{\gamma+1}{2\gamma}\frac{p_1'}{p_1}. \tag{7}$$

where p_1' is the acoustic pressure fluctuation upstream from the nozzle. Given that $\tau_{inj} \simeq 25$ ms << 140 ms and the interval of 3 s between interjection events which ensures sufficient time to damp acoustic oscillation, the downstream pipe termination can be treated as anechoic during the impulsive-injection phase. Using the aforementioned assumption, one finds that the downstream acoustic pressure p_2' is related to the acoustic velocity fluctuation, u_2', as follows:

$$p_2' = \rho_2 c_2 u_2' \tag{8}$$

where ρ_2 and c_2 are the averaged downstream density and speed of sound. The relative variation in mass-flow, $\dot{m}_2'/\dot{m}_2$, downstream from the nozzle, is given by

$$\begin{aligned}\frac{\dot{m}_2'}{\dot{m}_2} &= \frac{\rho_2'}{\rho_2} + \frac{u_2'}{u_2} \\ &= \frac{u_2'}{u_2}(1+M_2)\end{aligned} \tag{9}$$

where $M_2 \equiv u_2/c_2$ is the downstream Mach number. Since both the downstream and upstream Mach numbers are much smaller than one ($M_1 = u_1/c_1$ << 1 and M_2 << 1), Eq. (9) can be simplified to $\dot{m}_2'/\dot{m}_2 \simeq u_2'/u_2$, and one can take $T_1 \simeq T_2$, i.e., the temperatures in the down- and upstream sections to be approximately equal. Assuming quasi-steady behavior of the nozzle, one obtains the following direct-noise model:

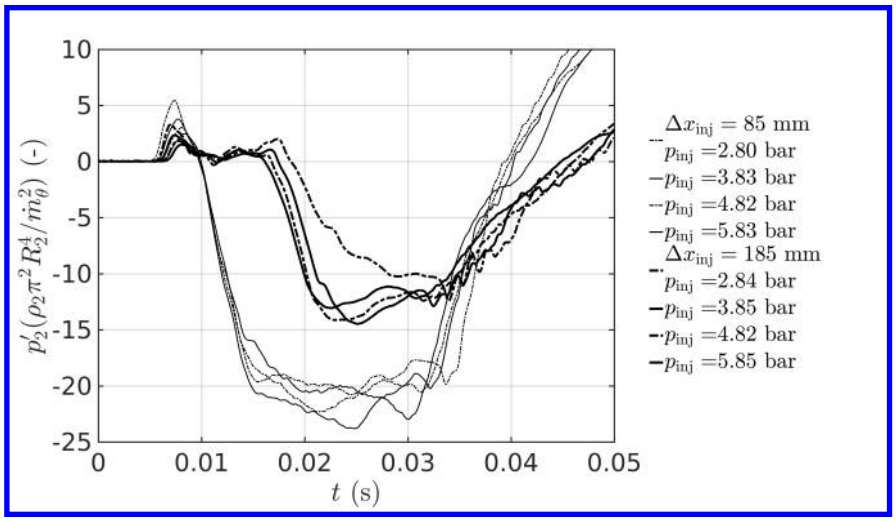

Fig. 4 Scaled downstream acoustic signal, p_2', due to unsteady swirl-nozzle interaction.

$$\begin{aligned} p_2' &= \rho_2 c_2 u_2' \\ &\simeq \frac{p_2}{p_1} c_2 u_2 \left(\frac{\gamma+1}{2}\right)\left(\frac{\dot{m}_{\rm inj}}{V_{\rm set}}\right)(t-t_0) \end{aligned} \tag{10}$$

where the ideal-gas relation $\rho_1 c_1^2 = \gamma p_1$ and Eq. (6) have been used.

In Fig. 3 (left-hand vertical axis), the dimensionless signal $p_2'/p_{\rm inj}$ generated by radial injection in the $\Delta x_{\rm inj}$ = 185 mm configuration is compared to the direct-noise model (Eq. (10)). One observes a strong initial positive pulse of direct sound corresponding to the opening of the valve at t_0 = 10 ms. The subsequent slow increase in p_2' is well predicted by Eq. (10) during the first 20 ms. This indicates that the signal is dominated by direct sound which is not related to the vorticity-nozzle interaction. The deviation for $t - t_0 > 20$ ms is due the limited low-frequency response of the microphone. N.b., the good predictive value of Eq. (10) indicates that any entropy-noise effects [1] which may have been caused by radial injection are negligible. Indeed, to derive the direct-noise model (Eq. (10)) adiabatic compression of the gas in the upstream reservoir and isentropic flow through the choked convergent-divergent nozzle were assumed.

In Fig. 3 (right-hand vertical axis) the dimensionless signal $\Delta p_2'/p_{\rm inj}$ of the difference in acoustic signal, $\Delta p_2' \equiv (p_2')_{\Delta x_{\rm inj}=85\ {\rm mm}} - (p_2')_{\Delta x_{\rm inj}=185\ {\rm mm}}$, due to radial injection in the $\Delta x_{\rm inj}$ = 85 mm and $\Delta x_{\rm inj}$ = 185 mm configurations is shown. A large part of the signals for $\Delta x_{\rm inj}$ = 85 mm and 185 mm is dominated by the direct sound discussed above. This effect is not dependent on the position of the injection point. Thus, this subtraction allows us to focus on the indirect sound generated by vorticity-nozzle interaction. One observes that after the first direct-sound pulse (positive peak at ca. 8 ms), there is a sudden dip in $\Delta p_2'/p_{\rm inj}$. This dip in the signal is believed to be due to the ingestion of main-flow oriented (axial) vorticity by the nozzle. After the valve is closed at $t \simeq 35$ ms, one observes an abrupt increase in $\Delta p_2'/p_{\rm inj}$. This increase is believed to be due to the increase in axial mass-flow rate through the nozzle after the main-flow oriented vorticity was evacuated. One notes that this sudden pressure increase, which occurs after the injection valve was closed, has almost the same amplitude as the initial dip upon opening of the valve. Experiments with longer injection times up to 120 ms showed the same increase in pressure p_2' when the valve was closed. The authors hypothesize that the unsteady radial mass injection forms two main-flow oriented vortices of opposite sign, viz., with net swirl of zero. Therefore, the sound generated by these vortices cannot be described in terms of S_D.

There is another major difference between the radial and tangential injection which remains to be elucidated. In the unsteady tangential-injection experiments, p_2' was proportional to the square of the injected mass-flow rate $\dot{m}_{\rm inj} = \dot{m}_\theta$. This is illustrated in Fig. 4 where the dimensionless downstream pressure signals $p_2'(\rho_2\pi^2 R_2^4/\dot{m}_\theta^2)$ obtained for a 25 ms tangential injection in the $\Delta x_{\rm inj}$ = 85 mm or $\Delta x_{\rm inj}$ = 185 mm configurations is shown. One observes a fair collapse of the data obtained for different $p_{\rm inj}$. Furthermore, one observes a sharp dip in p_2' upon ingestion followed by an increase in p_2' after evacuation of the axial vortex by the nozzle. The signal obtained for $\Delta x_{\rm inj}$ = 185 mm is very similar to the one obtained for $\Delta x_{\rm inj}$ = 85 mm. The delay of 8 ms between the two signal corresponds to the convective delay of

vortical structures over a distance of 100 mm by a uniform main flow of 12.5 m $\cdot$ s^{-1}, which is the mean flow velocity of the steady-background flow before tangential injection. This delay had already reported by Hirschberg et al. [6]. The difference in amplitude (a factor of 1.5) is due to viscous swirl decay as explained by Hirschberg et al. [6] For radial injection, the signal p_2' scales, by virtue of Eq. (5), linearly with $\dot{m}_{\text{inj}}$. In addition, one notes that the effect of the axial vorticity disappeared when the injection was performed at $\Delta x_{\text{inj}} = 185$ mm. The authors speculate that this is due to efficient turbulent mixing, which annihilates the two opposing-sign axial vortices formed during radial injection.

IV. Discussion and conclusion

Before coming to a final conclusion, it is important to rule out the possibility that radial injection produces a net swirl which significantly contributes to the response. As explained above, the acoustic signal p_2' for tangential injection is in first approximation proportional to the square of the swirl S_D. Using this scaling rule, one can estimate the swirl needed to obtain the signal observed after radial injection at $\Delta x = 85$ mm. One finds for a tangential-injection reservoir pressure $p_{\text{inj}} = 5.8$ bar a signal of $|p_2'|_{\text{amp}} \simeq 180$ Pa, while for the radial injection one observes $|p_2'|_{\text{amp}} \simeq 18$ Pa. To obtain the latter from a net swirl swirl $(S_D)_{\text{rad}}$ due to radial injection, one would have to assume that $(S_D)_{\text{rad}}$ be $\sqrt{18/180} = 0.31$ or 31% of the $(S_D)_{\text{tan}}$ created by means of tangential injection. For $p_{\text{inj}} = 2.8$ bar, the same assumptions require $(S_D)_{\text{rad}}$ to be $\sqrt{11/40} = 0.52$ or 52% of $(S_D)_{\text{tan}}$. The authors are confident that such a strong flow asymmetry can not be obtained by unsteady radial injection.

Thus, the authors trust that the results of impulsive radial-injection experiments are a consequence of the effects of main-flow oriented vorticity-nozzle interactions in the absence of a net swirl. The authors presented arguments which suggest that the response scales with the average of the square of the transversal velocity at the throat divided by square of the critical sound speed. This was verified for flows with a net swirl [11] and is expected to be more generally valid for the interaction of axially-oriented vorticity with a nozzle.

Acknowledgements

The presented measurements were carried out while Lionel Hirschberg was the beneficiary of a Deutsches Zentrum für Luft- und Raumfahrt (DLR) - Deutscher Akademischer Austauschdienst (DAAD) postdoctoral fellowship (no. 57424730). The authors thank Karsten Knobloch, Angelo Rudolphi, Sebastian Kruck, Oliver Klose, Nico Seiffert and Lech Modrzejewski for their support. Lionel Hirschberg thanks Aimee Morgans, Catherine Lemaitre and Assa Ashuach for their support.

References

[1] Morgans, A. S., and Duran, I., "Entropy Noise: A Review of Theory, Progress and Challenges," *Int. J. of Spray and Combust. Dyn.*, Vol. 8, No. 4, 2016, pp. 285–298. doi:10.1177/1756827716651791.

[2] Anthoine, J., Buchlin, J. M., and Hirschberg, A., "Effect of Nozzle Cavity on Resonance in Large SRM: Theoretical Modeling," *J. Propuls. and Power*, Vol. 18, No. 2, 2002, pp. 304–311. doi:10.2514/2.5935.

[3] Hirschberg, L., Hulshoff, S. J., Collinet, J., Schram, C., and Schuller, T., "Influence of Nozzle Cavity on Indirect Vortex- and Entropy-Sound Production," *AIAA J.*, Vol. 57, No. 7, 2019, pp. 3100–3103. doi:10.2514/1.J058138.

[4] Kings, N., and Bake, F., "Indirect combustion noise: noise generation by accelerated vorticity in a nozzle flow," *Int. J. Spray Combust. Dyn.*, Vol. 2, No. 3, 2010, pp. 253–266. doi:10.1260/1756-8277.2.3.253.

[5] Hirschberg, L., Bake, F., Knobloch, K., and Hulshoff, S. J., "Swirl-Nozzle Interaction Experiments: Influence of Injection-Reservoir Pressure and Injection Time," *AIAA J.*, Vol. 59, No. 7, 2021. doi:10.2514/1.J060291.

[6] Hirschberg, L., Hulshoff, S. J., and Bake, F., "Sound Production due to Swirl–Nozzle Interaction: Model-Based Analysis of Experiments," *AIAA J.*, Vol. 59, No. 4, 2021, pp. 1269–1276. doi:10.2514/1.J059669.

[7] Hirschberg, L., Bake, F., Knobloch, K., Rudolphi, A., Kruck, S., Klose, O., and Hulshoff, S. J., "Swirl-Nozzle Interaction Experiment: Quasi-Steady Model Based Analysis," *Experiments in Fluids*, Vol. 62, No. 8, 2021, pp. 1432–1114. doi: 10.1007/s00348-021-03271-y.

[8] Dutton, J. C., "Correlation of Nozzle Performance Degradation Due to Swirl," *J. Propuls. Power*, Vol. 5, No. 1, 1989, pp. 126–128. doi:10.2514/3.23125.

[9] Gany, A., Mor, M., and Goldman, C., "Analysis and Characteristics of Choked Swirling Nozzle Flows," *AIAA J.*, Vol. 43, No. 10, 2005, pp. 2177–2181. doi:10.2514/1.16887.

[10] van Holten, T., Heiligers, M., and Jaeken, A., "Choking Phenomena in a Vortex Flow Passing a Laval Tube: An Analytical Treatment," *J. Fluids Eng.*, Vol. 131, No. 4, 2009, p. 041201. doi:10.1115/1.3089532.

[11] Carpenter, P. W., "A General One-Dimensional Theory of Compressible Inviscid Swirling Flows in Nozzles," *Aeronautical Quarterly*, Vol. 27, No. 3, 1976, p. 201–216. doi:10.1017/S0001925900007708.

[12] Neuhaus, D., and Röhle, I., "Schnellschaltende Ventile für Anwendungen in der Luft und Raumfahrt," *Deutscher Luft- und Raumfahrtkongress*, 2006.